DOI: 10.1002/anie.201206715

Nanotubes

Microwave-Assisted Synthesis of Porous Ag_2S–Ag Hybrid Nanotubes with High Visible-Light Photocatalytic Activity**

Wenlong Yang, Lei Zhang, Yong Hu, Yijun Zhong, Hao Bin Wu, and Xiong Wen (David) Lou**

Heterostructures of semiconductors and noble metals have recently received much attention because of their unique optical, magnetic, electrical, and catalytic properties for different applications.[1–5] As an example, Yang and Ying recently designed different hybrid structures of Ag_2S–noble metals with optimized compositions and domain sizes with improved electrocatalytic activities.[6] Meanwhile, hollow micro/nanostructures with uniform morphology and good structural stability have also attracted considerable interest owing to their widespread applications in nanoreactors, drug delivery, gas sensors, and energy storage and conversion.[7,8] However, one-pot formation of heterostructures from distinct materials is difficult because of the dissimilar growth processes involved with different microscopic mechanisms and reaction rates.[9,10] Therefore, integrating different components to form complex hybrid nanostructures through facile procedures remains as a challenging but exciting topic in materials science.[11,12]

As one of the important semiconductor–noble metal heterostructures, Ag_2S–Ag nanohybrids have attracted great research interest owing to their excellent properties in photoelectric and medical devices, and photocatalysis.[13–15] Therefore, it is of great importance to develop a facile and rational strategy for the large scale preparation of well-defined Ag_2S–Ag heterostructures to explore their novel properties and applications.[16] Microwave-assisted synthesis is attractive and facile for rapid synthesis of nanocrystals with narrow particle-size distribution and high purity.[17–19] Herein, we report a facile strategy for one-pot formation of porous Ag_2S–Ag heterostructure nanotubes (HSNTs) by microwave-assisted surface sulfidation of Ag_2CO_3 nanorods (NRs). This process is facile and rapid, and only involves the reaction of Ag_2CO_3 NRs with thioacetamide (TAA) in ethanol under low intensity microwave irradiation (400 W) for 15 minutes (Figure 1). Moreover, the Ag content in the porous Ag_2S–Ag HSNTs can be easily tuned by varying synthesis parameters such as the TAA concentration. Different from conventional templating methods, the Ag_2CO_3 NRs in the present synthesis not only serve as the scaffold for the creation of hollow structures, but also are directly involved in the formation of the Ag_2S–Ag hybrids.

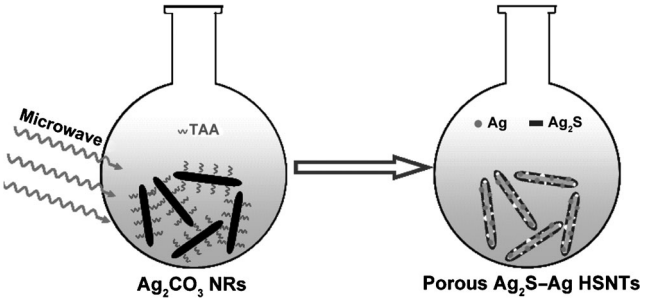

Figure 1. Illustration of the fabrication of porous Ag_2S–Ag HSNTs by a one-pot microwave-assisted method.

The as-prepared porous Ag_2S–Ag HSNTs were then evaluated as photocatalysts for both the degradation of methyl orange (MO) and the reduction of Cr^{VI} species in an aqueous solution under visible-light irradiation. Furthermore, the $^{\bullet}OH$ radicals formed in different Ag_2S–Ag photocatalysts were measured by the terephthalic acid fluorescence probe method, which revealed that the Ag content in the Ag_2S–Ag hybrids is crucial for obtaining optimized photocatalytic activity.

The reactions involved in the formation of Ag_2S–Ag hybrids under microwave irradiation might be described as follows.[20,21] First, under microwave irradiation TAA reacts with ethanol to form $CH_3(NH_2)C(OC_2H_5)$–SH [Eq. (1)], which further reacts to release H_2S [Eq. (2)].

$$CH_3CSNH_2 + C_2H_5OH \rightarrow CH_3(NH_2)C(OC_2H_5)\text{-}SH \quad (1)$$

$$CH_3(NH_2)C(OC_2H_5)SH + C_2H_5OH \rightarrow CH_3(NH_2)C(OC_2H_5)_2 + H_2S \quad (2)$$

Then, H_2S reacts quickly with Ag_2CO_3 at the surface of the Ag_2CO_3 NRs to produce a Ag_2S framework [Eq. (3)].

$$H_2S + Ag_2CO_3 \rightarrow Ag_2S + H_2O + CO_2 \quad (3)$$

Simultaneously, metallic Ag is produced by the thermal decomposition of Ag_2CO_3 under microwave irradiation

[*] W. L. Yang, Prof. Y. Hu, Y. J. Zhong
Key Laboratory of the Ministry of Education for Advanced Catalysis Materials, Institute of Physical Chemistry
Zhejiang Normal University, Jinhua, 321004 (P. R. China)
E-mail: yonghu@zjnu.edu.cn
Dr. L. Zhang, H. B. Wu, Prof. X. W. Lou
School of Chemical and Biomedical Engineering
Nanyang Technological University
70 Nanyang Drive, Singapore 637457 (Singapore)
E-mail: xwlou@ntu.edu.sg
Homepage: http://www.ntu.edu.sg/home/xwlou

[**] Y.H. greatly acknowledges the financial support from the Natural Science Foundation of China (21171146) and Zhejiang Provincial Natural Science Foundation of China (Y4110304).

Supporting information for this article is available on the WWW under http://dx.doi.org/10.1002/anie.201206715.

[Eq. (4)]).[22]

$$Ag_2CO_3 \rightarrow 2\,Ag + {}^1/_2\,O_2 + CO_2 \quad (4)$$

The key to the successful synthesis of porous Ag_2S–Ag HSNTs by a one-pot microwave-assisted method in the present system is to retain the structure of the Ag_2CO_3 NR templates. As Ag_2CO_3 can dissolve in hot water, only agglomerates of Ag_2S–Ag hybrids (Figure S1, see the Supporting Information) are obtained by the microwave-assisted in situ surface sulfidation process with water as the solvent. Thus, a nonaqueous solvent, such as ethanol as we have chosen for this work, should be used for the microwave-assisted synthesis. Additionally, the concentration of TAA in this synthesis is also an important parameter to retain the structural integrity of the as-prepared porous Ag_2S–Ag HSNTs and control the content of metallic Ag in the HSNTs. Samples prepared with 0, 1.8, 3.5, 5.4, and 7.0 mM concentrations of TAA are denoted as pure Ag, H-1, H-2, H-3, and pure Ag_2S, respectively.

The crystallographic structure and phase purity of the as-prepared porous Ag_2S–Ag HSNTs was examined by X-ray powder diffraction (XRD), and the typical result from the sample H-2 ($C_{TAA} = 3.5$ mM) is shown in Figure 2. The diffraction peaks marked by triangles can be assigned to

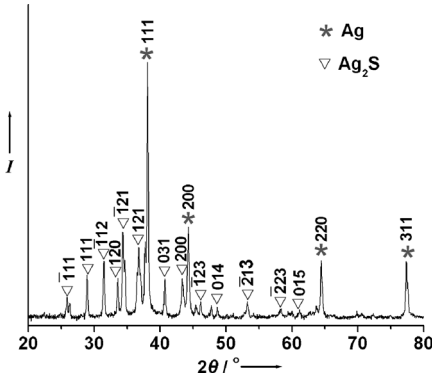

Figure 2. XRD pattern of the as-prepared porous Ag_2S–Ag HSNTs ($C_{TAA} = 3.5$ mM).

monoclinic Ag_2S (JCPDS card no. 77-0072; space group: $P2_1/n$, $a = 4.229$ Å, $b = 6.931$ Å, and $c = 9.091$ Å), and those marked by asterisks correspond to face-centered cubic Ag (JCPDS card no. 87-0720; space group: $Fm\bar{3}m$, $a = b = c = 4.077$ Å). The result of XRD analysis suggests the successful conversion from Ag_2CO_3 NRs to Ag_2S–Ag hybrids by this one-pot microwave-irradiation method. No additional peaks were detected, thus indicating the high purity of the sample. In addition, the XRD patterns of the as-prepared Ag_2CO_3 NRs and other samples obtained with different TAA concentrations are shown in Figure S2 (see the Supporting Information). These results indicate that the TAA concentration in the microwave-assisted synthesis can be used to tune the content of metallic Ag in the hybrids. Thus, only pure Ag is obtained in the absence of TAA, whereas a sufficient amount of TAA in the synthesis results in the formation of pure Ag_2S.

Scanning electron microscope (SEM) and transmission electron microscope (TEM) characterizations provide insights into the morphology and detailed structure of the as-prepared Ag_2CO_3 NR templates and the porous Ag_2S–Ag HSNTs. A panoramic view of the as-prepared Ag_2CO_3 NRs templates (Figure 3a) reveals that the sample is entirely composed of uniform nanorods about 100–150 nm in diameter and 1–2 μm in length. Figure 3b shows the SEM image of

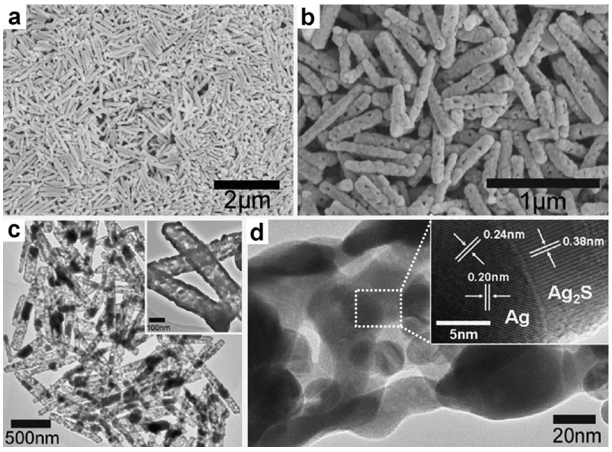

Figure 3. SEM images of the as-prepared a) Ag_2CO_3 NRs, b) porous Ag_2S–Ag HSNTs; TEM images of c) porous Ag_2S–Ag HSNTs (inset: a high-magnification image. Scale bar: 100 nm); d) a section of a single HSNT (inset: corresponding HRTEM image. Scale bar: 5 nm).

porous Ag_2S–Ag HSNTs formed by the one-pot microwave-assisted synthesis (sample H-2; $C_{TAA} = 3.5$ mM). The well-defined Ag_2CO_3 NRs are fully converted into porous Ag_2S–Ag HSNTs without any impurity particles or aggregates. The Ag/S ratio determined by energy dispersive X-ray spectrometry (EDS) analysis is around 3.6 (see the Supporting Information, Figure S3 and Table S1), which suggests the Ag_2S/Ag molar ratio of 0.64 in the porous Ag_2S–Ag HSNTs. The EDS analysis also indicates that the Ag_2S/Ag molar ratio in the product increases when the concentration of TAA in the synthesis is increased (see the Supporting Information, Table S1). The geometrical structure and hollow interior of as-prepared porous Ag_2S–Ag HSNTs were further elucidated by TEM results. Figure 3c shows the incorporation of Ag nanocrystals into the porous Ag_2S framework, and the resultant porous tubes well duplicate the size and shape of the Ag_2CO_3 NRs templates. The interior void and the porous shell indicate that the Ag_2CO_3 NRs are fully converted into porous Ag_2S–Ag HSNTs after microwave irradiation for 15 minutes. Figure 3d displays a TEM image of a section of a single HSNT, and the heterojunction region between Ag_2S and Ag is clearly shown in the HRTEM image (inset). We also observed that the size of the primary Ag and Ag_2S nanocrystals in the HSNTs is relatively big. As a result, the Brunauer—Emmet–Teller (BET) specific surface area of the H-2 sample is only about 12.9 $m^2\,g^{-1}$. The spatial distribution

of the composition in a single HSNT was further studied by elemental mapping. The mapping result shows uniform distribution of Ag and S throughout the HSNT (see the Supporting Information, Figure S4).

In the present strategy, a layer of Ag_2S is first generated on the surface of Ag_2CO_3 NRs by the microwave-assisted in situ sulfidation process. This Ag_2S layer should improve the structural stability and reduce the impact of released O_2 and CO_2 gases owing to the thermal decomposition of Ag_2CO_3. As a result, almost no structural deformation, collapse or obvious shrinkage, is found in the resultant hybrid hollow structures. For comparison, the SEM image of the pure Ag nanoparticles obtained by directly irradiating Ag_2CO_3 templates in the absence of TAA for 15 minutes apparently reveals the collapse of the nanorod structure (see the Supporting Information, Figure S5a). On the other hand, with more TAA present in the synthesis, the structure of the nanotubes can be better retained (see the Supporting Information, Figure S5b–d). Surface information of the porous Ag_2S–Ag HSNTs was further acquired with the X-ray photoelectron spectroscopy (XPS; see the Supporting Information, Figure S6) technique. The peaks at 368.2 and 374.2 eV in the Ag 3d photoelectron spectrum (in Figure S6b) are in good agreement with the binding energies of Ag $3d_{5/2}$ and Ag $3d_{3/2}$ of the metallic Ag^0. Meanwhile, the peaks at 367.8 and 373.8 eV could be assigned to Ag $3d_{5/2}$ and Ag $3d_{3/2}$ of Ag^+ ions in the Ag_2S HSTNs.[13] Thus, the presence of both metallic state (Ag^0) and Ag^+ ions in the Ag_2S–Ag HSNTs is again confirmed.

Recent studies have suggested that Ag_2S–Ag heterostructures might possess advantages such as favorable charge transfer from Ag to Ag_2S and a wide absorbance range of light.[16] Thus, this new type of porous HSNTs was investigated as a promising photocatalyst in the present work. Figure 4 shows the photocatalytic activities of the as-prepared porous Ag_2S–Ag HSNTs, which were evaluated for the degradation of organic dye MO and the reduction of aqueous Cr^{VI} under visible-light irradiation. Figure 4a presents the visible-light photodegradation behaviors of MO using pure Ag_2S and porous Ag_2S–Ag HSNTs that were obtained with different concentrations of TAA as photocatalysts, and commercial Degussa P25 nanoparticles for comparison. C is the concentration of MO after light irradiation for a certain period, and C_o is the concentration of the MO after reaching adsorption/desorption equilibrium in dark. After irradiation of 30 min, nearly 92.1% of the MO is degraded by the sample H-2, whereas other samples including pure Ag_2S, P25, H-1 and H-3 exhibit lower activities with degradation rates of about 7.8%, 25.4%, 13.9%, and 82.5%, respectively. Figure 4b displays the photocatalytic reduction of Cr^{VI} catalyzed by pure Ag_2S, P25, and different porous Ag_2S–Ag HSNTs under visible-light illumination. Similarly, the sample H-2 exhibits the highest photocatalytic activity among the five samples. We have further studied the stability and reusability of the photocatalyst by collecting and reusing the same photocatalysts for 5 cycles (see the Supporting Information, Figure S7). The results show that there is only neglible loss of the photocatalytic activity; this loss might be partly caused by the loss of the photocatalysts during each collection and rinsing step.

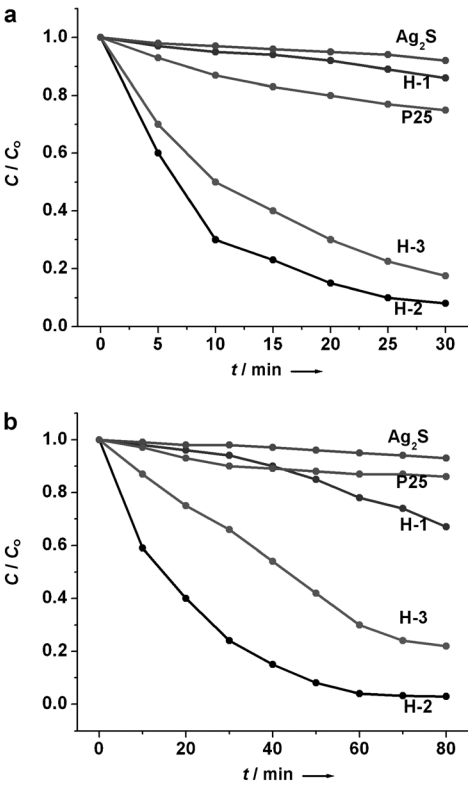

Figure 4. a) Photocatalytic degradation of MO, and b) photocatalytic reduction of Cr^{VI} in the presence of different photocatalysts. C is the concentration of MO after light irradiation for a certain period, and C_o is the concentration of the MO after reaching adsorption/desorption equilibrium in dark.

The superior photocatalytic performance of the porous Ag_2S–Ag HSNTs may be ascribed to the enhanced charge-transfer process in the hybrid nanostructures. The work function of Ag and the bottom of the conduction band of Ag_2S are 4.26 and 4.42 eV, respectively, relative to the vacuum energy level.[23] Therefore, the photoexcited electrons in the conduction band of Ag_2S can transfer to Ag in the hybrid nanostucture easily. The induced charge separation could suppress the recombination of excited electrons and holes, and hence increasing the photocatalytic activity.[13] However, excess Ag content may reduce the catalytic efficiency of the Ag_2S–Ag HSNTs owing to the reduced availability of the semiconductor surface for light absorption and pollutant adsorption.[24] As a result, the sample H-2 photocatalyst with a moderate Ag_2S/Ag molar ratio exhibits superior activity over other samples.

Furthermore, the $^{\bullet}OH$ radicals formed in different porous HSNTs and pure Ag_2S photocatalysts could be probed using a method described previously.[25] It is well known that $^{\bullet}OH$ reacts with terephthalic acid (TA) in basic solution to generate 2-hydroxy-terephthalic acid (TAOH), which emits a unique fluorescence signal with the peak centered at 426 nm.[26] Significant fluorescent signals associated with TAOH are generated upon visible-light irradiation of the different photocatalysts suspended in a TA solution for 10 minutes (Figure 5). It is clearly demonstrated that the photoexcited holes are powerful enough to oxidize surface-

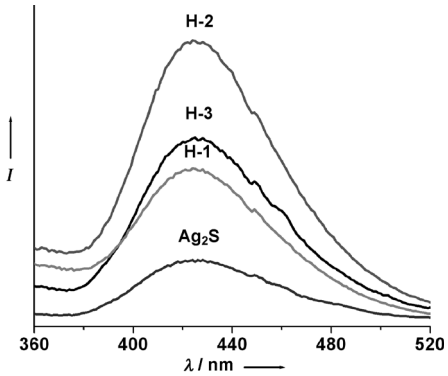

Figure 5. Fluorescence spectra of TAOH formed by the reaction of TA with ·OH radicals generated from different samples under visible-light irradiation for 10 min.

adsorbed hydroxy groups and water molecules to generate ·OH radicals. Additionally, the maximum number of ·OH radicals is formed by using the sample H-2 photocatalyst in the photoreaction process; this result is in good agreement with results of photodegradation of MO and photoreduction of Cr^{VI}. Therefore, the excellent visible-light-driven photocatalytic activity seen for the H-2 photocatalyst might be due to the presence of a suitable amount of Ag, which improves separation and migration of the photogenerated electrons and holes, thus allowing both the electrons and holes to participate in the overall photocatalytic reaction.

In summary, we have rationally developed a facile one-pot microwave-assisted method to synthesize porous Ag_2S–Ag heterostructure nanotubes with uniform morphology and good structural stability. The as-prepared hybrid structures manifest excellent photocatalytic activity for degradation of MO and reduction of aqueous Cr^{VI}. Furthermore, the optimal synergistic effect between Ag_2S and Ag has been investigated through the generation of ·OH radicals in different hybrid photocatalysts. This work represents a good example of fabricating nanostructured materials using the facile microwave-assisted method. The versatile approach demonstrated in the present work could potentially be extended to synthesize other hybrid hollow nanostructures for different applications.

Received: August 20, 2012
Published online: October 11, 2012

Keywords: microwave chemistry · nanotubes · photochemistry · semiconductors · silver

[1] S. J. Hurst, E. K. Payne, L. D. Qin, C. A. Mirkin, *Angew. Chem.* **2006**, *118*, 2738; *Angew. Chem. Int. Ed.* **2006**, *45*, 2672.
[2] D. J. Milliron, S. M. Hughes, Y. Cui, L. Manna, J. B. Li, L. W. Wang, A. P. Alivisatos, *Nature* **2004**, *430*, 190.
[3] T. Mokari, E. Rothenberg, I. Popov, R. Costi, U. Banin, *Science* **2004**, *304*, 1787.
[4] D. Seo, C. Il Yoo, J. Jung, H. Song, *J. Am. Chem. Soc.* **2008**, *130*, 2940.
[5] Y. Jung, D. K. Ko, R. Agarwal, *Nano Lett.* **2007**, *7*, 264.
[6] J. Yang, J. Y. Ying, *Angew. Chem.* **2011**, *123*, 4733; *Angew. Chem. Int. Ed.* **2011**, *50*, 4637.
[7] X. W. Lou, L. A. Archer, Z. C. Yang, *Adv. Mater.* **2008**, *20*, 3987.
[8] L. Zhang, L. Zhou, H. B. Wu, R. Xu, X. W. Lou, *Angew. Chem.* **2012**, *124*, 7379; *Angew. Chem. Int. Ed.* **2012**, *51*, 7267.
[9] C. L. Yan, L. Nikolova, A. Dadvand, C. Harnagea, A. Sarkissian, D. F. Perepichka, D. F. Xue, F. Rosei, *Adv. Mater.* **2010**, *22*, 1741.
[10] R. D. Robinson, B. Sadtler, D. O. Demchenko, C. K. Erdonmez, L. W. Wang, A. P. Alivisatos, *Science* **2007**, *317*, 355.
[11] W. L. Yang, Y. Liu, Y. Hu, M. J. Zhou, H. S. Qian, *J. Mater. Chem.* **2012**, *22*, 13895.
[12] Q. Zhang, W. S. Wang, J. Goebl, Y. D. Yin, *Nano Today* **2009**, *4*, 494.
[13] M. L. Pang, J. Y. Hu, H. C. Zeng, *J. Am. Chem. Soc.* **2010**, *132*, 10771.
[14] Y. Zhang, G. S. Hong, Y. J. Zhang, G. C. Chen, F. Li, H. J. Dai, Q. B. Wang, *ACS Nano* **2012**, *6*, 3695.
[15] V. M. Huxter, T. Mirkovic, P. S. Nair, G. D. Scholes, *Adv. Mater.* **2008**, *20*, 2439.
[16] F. R. Jiang, Q. W. Tian, M. H. Tang, Z. G. Chen, J. M. Yang, J. Q. Hu, *CrystEngComm* **2011**, *13*, 7189.
[17] M. Baghbanzadeh, L. Carbone, P. D. Cozzoli, C. O. Kappe, *Angew. Chem.* **2011**, *123*, 11510; *Angew. Chem. Int. Ed.* **2011**, *50*, 11312.
[18] Y. Hu, Y. Liu, H. S. Qian, Z. Q. Li, J. F. Chen, *Langmuir* **2010**, *26*, 18570.
[19] Y. Liu, L. Zhou, Y. Hu, C. F. Guo, H. S. Qian, F. M. Zhang, X. W. Lou, *J. Mater. Chem.* **2011**, *21*, 18359.
[20] Y. Hu, H. H. Qian, Y. Liu, G. H. Du, F. M. Zhang, L. B. Wang, X. Hu, *CrystEngComm* **2011**, *13*, 3438.
[21] Y. Liu, Y. Hu, C. F. Guo, X. Hu, *J. Am. Ceram. Soc.* **2011**, *94*, 1667.
[22] W. S. Epling, G. B. Hoflund, G. N. Salaita, *J. Phys. Chem. B* **1998**, *102*, 2263.
[23] B. Levy, *Photochemical Conversion and Storage of Solar Energy*, Springer, New York, **1990**.
[24] I. M. Arabatzis, T. Stergiopoulos, D. Andreeva, S. Kitova, S. G. Neophytides, P. Falaras, *J. Catal.* **2003**, *220*, 127.
[25] Y. Liu, Y. Hu, M. J. Zhou, H. S. Qian, X. Hu, *Appl. Catal. B* **2012**, *125*, 425.
[26] G. Liu, P. Niu, L. C. Yin, H. M. Cheng, *J. Am. Chem. Soc.* **2012**, *134*, 9070.

